Cellular automaton model of chemical wave propagation on fractals

Andrew J. Irwin and Simon J. Fraser
Scarborough College and Department of Chemistry, University of Toronto, Toronto, Ontario, M5S 1A1, Canada

(Received 25 April 1990; accepted 22 May 1990)

A three-state cellular automaton (CA) model of nucleation and chemical wave propagation on fractal lattices is discussed. In the CA, seeds produce spreading wavefronts of active or transformed sites which mutually annihilate on collision. Many chemical and biological growth processes display this behavior. Pattern formation and growth from isolated seeds and from random initial distributions of seeds are considered. Steady-state behavior for continuous seeding is also discussed. For isolated seeds, surface and volume growth exponents on fractals do not show the simple relation that holds for homogeneous lattices, and lattice topology plays an important dynamical role. For initial seeding, mean-field theory predicts that growth depends on the fractal dimension D (since the minimum path dimension is one). However the fractal gap hierarchy (lacunarity) introduces fluctuation contributions. For continuous seeding entirely new effects arise. On sponge-like fractals oscillators are created; these eventually fill the lattice even at low seeding density. However tree-like fractals cannot support oscillators, and instead exhibit dynamical scaling behavior. For mixed fractals complicated periodic phenomena can arise.

I. INTRODUCTION

There is an interesting connection between nucleation processes[1] and the spreading of chemical waves[2] in random or homogeneous media. In nucleation, one phase grows from random seeds into another as a system of (spherical) propagating fronts. But the *surface* of the growing phase can also represent the active wavefront spreading through a quiescent field in an excitable medium, e.g., wave propagation in the Belousov–Zhabotinksky (BZ) reaction.[2-4] In such processes the excited state returns to quiescence through a refractory state.

In this study, we will exploit this connection by relating surface and volume growth, and by relating mean-field theories of nucleation in homogeneous media to far more erratic growth phenomena in random media. Specifically, wavefront propagation (the dynamical part of the model) is imitated by a cellular automaton (CA),[5] and the random medium (the static part) is modeled by a fractal lattice[6] of variable structure.

Biologically, this model describes the spread of viral or fungal infection, in complicated spaces like the lungs or central nervous system or tree bark.[7] For example, rabies (which has no viremia) spreads in this way by propagating along nerve fibers from the point of infection. The model is an epidemic process,[8] with sure infection of neighbors, on a fractal of variable dimension and connectedness. *Chemically*, the model represents tarnishing reactions on a spongy catalyst[9] or wave propagation on percolation clusters of catalytic beads, e.g., the BZ reaction on ferroin impregnated beads.[10] Nucleation examples of such processes are characterized by sharp, dispersionless fronts of activity, which can leave a damaged or transformed region in their wake. Wave propagation examples show a variety of effects depending on the history and structure of the medium.

Propagation of the active front is imitated by a three-state cellular automaton (CA)[11] defined as follows: Cells (sites) on the lattice can be in one of three states, Q (quiescent), A (active), or R (refractory). The CA rule through one time step is

$$\begin{aligned} &\text{Q (neighboring A)} &&\rightarrow \text{A},\\ &\text{A} &&\rightarrow \text{R},\\ &\text{R} &&\rightarrow \text{Q},\\ &\text{Q (not neighboring A)} &&\rightarrow \text{Q}, \end{aligned} \tag{1.1}$$

where all lattice sites are updated simultaneously. Neighborhood is specified by the square-matching-lattice topology: Any "corner" or "edge" site of a given site is a neighbor. A variety of behavior is displayed by this CA, but characteristically active waves spread out from (random) seeds and annihilate on collision.

The underlying fractal lattice, $\mathcal{F}$ say, is generated by decimation of the square, using Vicsek snowflake ($\mathcal{S}$), Sierpinski carpet ($\mathcal{C}$), and square ($\mathcal{L}$) generators.[12] The fractal dimension[6,13] D and connectedness[14] of the fractal can be altered by changing generator probabilities, $p_{\mathcal{S}}$, etc., so that random fractal percolation clusters, with any $D \in [\log_3 5, 2]$ can be produced. Since CA neighborhood and lattice connectedness have identical local topologies, the CA always propagates on any realization of $\mathcal{F}$. An important simplifying feature of $\mathcal{F}$ is that the minimum path exponent[15] $d_{\min}$ is one (as measured in first-passage-time simulations) and so D equals d_{chem}, the chemical dimension, because

$$d_{\text{chem}} = D/d_{\min}. \tag{1.2}$$

Dimension d_{chem} controls the growth of area swept out by fronts spreading at fixed velocity on $\mathcal{F}$.[16] Therefore the simplest possible growth law depends on D alone.

The reference dynamical picture is provided by the mean-field theory of *continuous* nucleation and growth.[17-19] In this picture, surface wavefronts of A sites grow outwards at constant velocity v, and the volume fraction, f say, swept

 0021-9606/90/173471-13$03.00

out by the *first passage* of A is given by

$$f(t) = 1 - \exp\left(-\frac{Kt^{d+1}}{d+1}\right). \tag{1.3}$$

Here d is the Euclidean dimension of the supporting space or lattice, and K is a shape-dependent constant proportional to v^d and the seeding rate. For initial seeding[20,21] at $t = 1$ the volume swept out by the first passage of A is given by

$$f(t) = 1 - \exp(-Kt^d). \tag{1.4}$$

The surface population of A for these different seeding models is given by the time derivatives of Eqs. (1.3) and (1.4). Even in standard lattice geometries the region occupied by A and its surface may have a complicated topology.[22,23]

Provided initial seeding is random (Poisson) and the medium is homogeneous, *mean-field* equations like (1.3) and (1.4) (and their time derivatives) describe population dynamics *exactly*. However, in an inhomogeneous medium deviations from mean-field theory occur, and these are most pronounced for processes whose length scale is below the maximum gap size. Therefore such deviations persist in some sense at all length and time scales in a fractal medium where the correlation length (gap size) is infinite.[6]

Lattice structure also plays a crucial role in the continuous seeding of an excitable medium,[24] where new seeds form in regions which have been repeatedly swept by active waves. (This contrasts with the irreversible behavior of simple nucleation.) The CA may produce expanding, self-sustaining patterns or (where such patterns cannot form) dynamical scaling of essentially transient steady-state patterns.

In Sec. II we briefly discuss the construction and characterization of the continuously variable fractal lattices that are used as a supporting medium.

In Sec. III we discuss single-site growth showing how growth exponent anomalies arise on fractals. Details of time evolution are also related to connectedness and (discrete) scaling; the difference in propagation on tree-like and sponge-like fractals is apparent.[14]

In Sec. IV we discuss growth for initial seeding, where nucleation and wave propagation are related in a simple way. On fractals, fluctuations are again important, and the role of lacunarity (gap structure) is discussed. Growth displays a continuous dynamical symmetry on sponges but a discrete symmetry on trees. We present simulation and exact enumeration results confirming this.

In Sec. V we describe time evolution of continuously seeded chemical waves on fractals, showing how the response of the medium depends on fractal structure. A nonlinear Markov chain model accurately describes behavior at high seeding density. At low seeding density this model also applies to the self-sustaining patterns that form on sponge-like fractals and homogeneous lattices. A dynamical scaling theory is discussed for the transient patterns that form on tree-like fractals at low seeding density; such patterns self-destruct if seeding stops. The rich variety of self-sustaining states that arise when seeding is interrupted is also mentioned.

In Sec. VI we summarize our results and discuss their implications.

II. VARIABLE FRACTAL MEDIUM FOR CA GROWTH

The algorithm for generating connected fractal lattices to support CA growth has been described in Ref. 12. It uses recursive decimation of square elements by mixing two or more generators to produce a lattice $\mathcal{F}$ of well defined fractal dimension D. If we mix the Vicsek snowflake ($\mathcal{S}$), Sierpinski carpet ($\mathcal{C}$), and square-matching-lattice ($\mathcal{L}$) generators we can produce a "planar" fractal medium with any D between $D_{\mathcal{S}} = \log 5/\log 3$ and $D_{\mathcal{L}} = 2$. In particular, we can generate lattices of the same D but different connectedness by mixing generators. In this study we use lattices decimated to level $l = 3,4$, and 5. If

$$\text{Prob}\{\mathcal{S}\} = p_{\mathcal{S}}, \quad \text{Prob}\{\mathcal{C}\} = p_{\mathcal{C}},$$
$$\text{and } \text{Prob}\{\mathcal{L}\} = p_{\mathcal{L}} = 1 - p_{\mathcal{S}} - p_{\mathcal{C}}, \tag{2.1}$$

then

$$D = D(p_{\mathcal{S}}, p_{\mathcal{C}}) = \frac{\log \mu(p_{\mathcal{S}}, p_{\mathcal{C}})}{\log \lambda} = \frac{\log[5p_{\mathcal{S}} + 8p_{\mathcal{C}} + 9(1 - p_{\mathcal{S}} - p_{\mathcal{C}})]}{\log 3}, \tag{2.2}$$

where μ is the mass scale factor and λ ($= 3$) is the length scale factor for $\mathcal{F}$. We can plot D as a function of $p_{\mathcal{S}}$, $p_{\mathcal{C}}$, and $p_{\mathcal{L}}$ as a three-component mixture.[25] The contours of constant D are found from the equation

$$\frac{\partial D}{\partial p_{\mathcal{S}}} \delta p_{\mathcal{S}} + \frac{\partial D}{\partial p_{\mathcal{C}}} \delta p_{\mathcal{C}} = 0, \tag{2.3}$$

which, from Eq. (2.2), reduces to

$$\frac{-4}{\mu \log 3} \delta p_{\mathcal{S}} + \frac{-1}{\mu \log 3} \delta p_{\mathcal{C}} = 0. \tag{2.4}$$

The contour corresponding to $D = D_{\mathcal{C}}$ contours are shown in Fig. 1, and three mixtures: (a), (b), and (c) with this dimension are indicated. From Eq. (2.4), all other constant

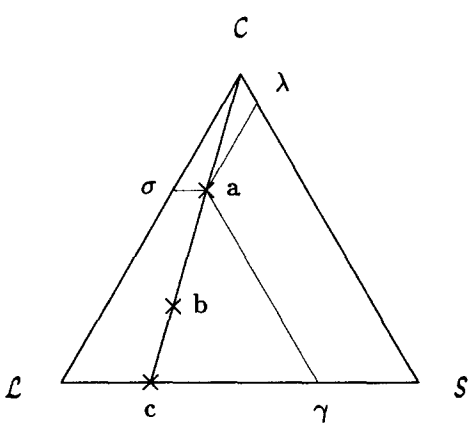

FIG. 1. The triangle with unit sides shows the mixture space for three fractal generators. The vertices $\mathcal{S}$, $\mathcal{C}$, and $\mathcal{L}$ correspond to pure snowflake, carpet and square-matching lattice, respectively. All lattice configurations on the line from vertex $\mathcal{C}$ to edge $\mathcal{L}\mathcal{S}$ correspond to the fractal dimension $D = D_{\mathcal{C}} = \log 8/\log 3$. All contours for any constant D are parallel to this line. Three mixtures with $D = D_{\mathcal{C}}$ are marked: (a) at $p_{\mathcal{C}} = 5/8$, (b) at $p_{\mathcal{C}} = 1/4$, and (c) at $p_{\mathcal{C}} = 0$. Realizations for $l = 4$ are shown in Fig. 2. For mixture (a), the corresponding generator probabilities are indicated by the thin lines: $a\sigma = p_{\mathcal{S}}$, $a\gamma = p_{\mathcal{C}}$, and $a\lambda = p_{\mathcal{L}}$.

contours are parallel to this $D_{\mathscr{C}}$ line. For mixture (a) we have drawn the component probabilities: $a\sigma$ for $\mathscr{S}$, $a\gamma$ for $\mathscr{C}$, and $a\lambda$ for $\mathscr{L}$. Realizations for mixtures (a), (b), and (c) with $D = D_{\mathscr{C}} = \log 8/\log 3$ are shown in Fig. 2. In general, the tree-like or sponge-like character[14] (connectedness) depends on generator probabilities.

III. GROWTH FROM SINGLE SITES ON FRACTALS

Growth from isolated seeds is now examined: On fractals even this simple process shows deviations from mean-field behavior. Fractal dimension D is often estimated by counting the number of sites at Euclidean distance r from an arbitrary site $\mathbf{r}$ say; this number increases like r^D. Similarly, if $d_{\min} = 1$, the neighborhood $|\mathscr{N}(\mathbf{r},t)|$ swept out at time t increases like t^D, so CA propagation provides a dynamical way of measuring D. Because $\mathscr{N}(\mathbf{r},t)$ is the union of successive "rings" of activity $\mathscr{A}(\mathbf{r},s)$, therefore

$$N(\mathbf{r},t) = |\mathscr{N}(\mathbf{r},t)| = \sum_{s=1}^{t} |\mathscr{A}(\mathbf{r},s)| = \sum_{s=1}^{t} A(\mathbf{r},s), \tag{3.1}$$

where $|\cdots|$ denote the number of elements in a set.[26] Mean-field theory then predicts that boundary population $A(\mathbf{r},t)$ should increase (smoothly) as t^{D-1}. However we will see that this need not be true on fractals because of the infinite correlation length of spatial fluctuations.

The predictability of growth is related to connectedness: On the snowflake (a tree), the spread of excitation is simplified by its quasi-one-dimensional structure, i.e., there is only one path between any two lattice points. Counting the number of neighbors of any lattice site can be done recursively or by exact enumeration using lattice symmetry, but since decimation creates new neighborhood topologies as the decimation level l increases, this recursive counting requires small, continuous modifications.[27] In contrast, on sponge-like fractals like the carpet, counting neighborhoods of a given radius is difficult because the number of distinct topologies grows very rapidly with l, so a simple recursive algorithm does not exist.[28] However, lattice averages are better approximated by continuous scaling on sponges because fluctuations cancel. We illustrate these statements with calculations for seeds at corner sites.

First we develop a formalism for the growth exponent in the number of boundary sites of any lattice neighborhood. Because growth is not a stationary process,[29-31] we define an instantaneous "surface" (or boundary site) growth exponent $\alpha(\mathbf{r},t)$ for the site at $\mathbf{r}$ at time t by

$$\alpha(\mathbf{r},t) = \log_t A(\mathbf{r},t). \tag{3.2}$$

where, to be precise, $A(\mathbf{r},t)$ is the number of active sites at time t that have evolved from a seed at $\mathbf{r}$ at $t = 1$. Then we define the distribution function F of α by

$$F(\alpha;\mathbf{r},t) = \frac{1}{t} \sum_{s=1}^{t} \theta\,[\alpha - \log_s A(\mathbf{r},s)\,], \tag{3.3}$$

where θ is the Heaviside function. Using F as integrator[32] we can define moments of α by

$$\overline{\alpha^m(\mathbf{r},t)} = \int_0^\infty \alpha^m\, dF(\alpha;\mathbf{r},t). \tag{3.4}$$

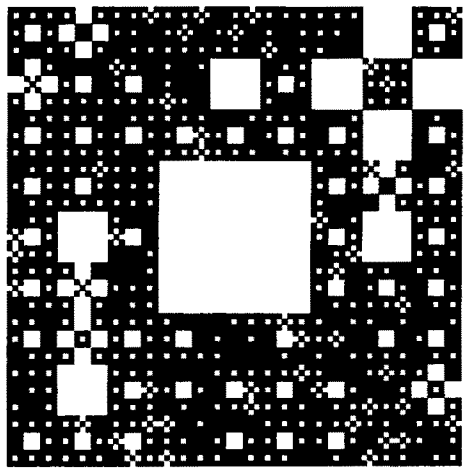

(a)

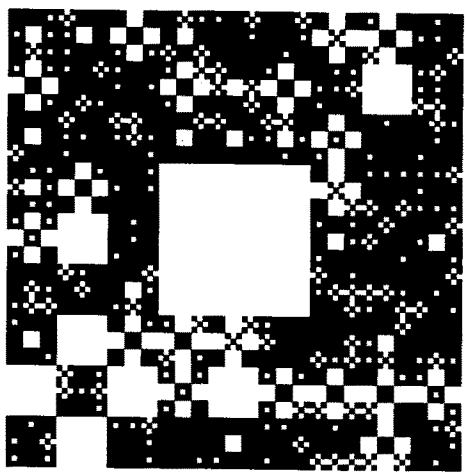

(b)

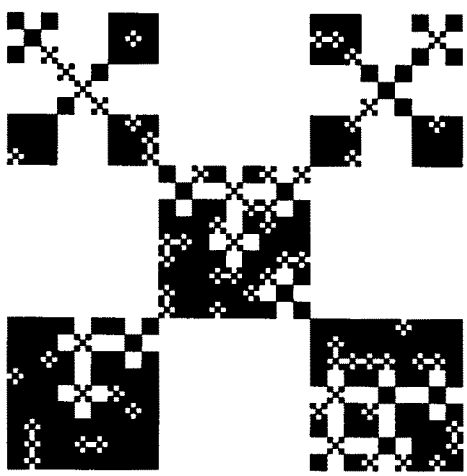

(c)

FIG. 2. Figure shows random fractal lattices grown at compositions giving the carpet fractal dimension $D_{\mathscr{C}} = \log 8/\log 3$. The mixtures are: (a) $p_{\mathscr{S}} = 3/32, p_{\mathscr{C}} = 5/8, \quad p_{\mathscr{L}} = 9/32;$ (b) $p_{\mathscr{S}} = 3/16, \quad p_{\mathscr{C}} = 1/4, p_{\mathscr{L}} = 9/16;$ (c) $p_{\mathscr{S}} = 1/4, p_{\mathscr{C}} = 0, p_{\mathscr{L}} = 3/4$. The carpet component decreases from vertex $\mathscr{C}$ to edge $\mathscr{L}\mathscr{S}$ along the $D = D_{\mathscr{C}}$ line in Fig. 1.

Lattice averages $\langle \cdots \rangle$ of these moments are defined in the usual way as

$$\langle \overline{\alpha^m(\mathbf{r},t)} \rangle = \int_0^\infty \alpha^m \, d\langle F(\alpha;\mathbf{r},t)\rangle$$
$$= \int_0^\infty \alpha^m \, d\left[\frac{1}{|\mathscr{F}|}\sum_{\mathbf{r}\in\mathscr{F}} F(\alpha;\mathbf{r},t)\right]. \quad (3.5)$$

We can calculate $\overline{\alpha}$ for the corner site $\mathbf{r}_c$ of the snowflake as follows. A lower bound $\alpha_b(\mathbf{r}_c,3^j)$ at times 3^j ($j=1,2,\ldots$) is given by

$$\alpha_b(\mathbf{r}_c,3^j) = \frac{1}{3^j}\sum_{s=1}^{3^j}\frac{\log A(\mathbf{r}_c,s)}{\log 3^j} = \frac{1}{3^j\log 3^j}\log\prod_{s=1}^{3^j} A(\mathbf{r}_c,s)$$
$$= \frac{1}{3^j j\log 3}\log 3^{\beta^{j-1}} = \frac{1}{3}, \quad (3.5)$$

exactly for all j. Similarly an upper bound $\alpha_B(\mathbf{r}_c,3^j)$ at times 3^j can be calculated by summing the contribution from successive time intervals $[3^{j-1},3^j]$. This gives

$$\alpha_B(\mathbf{r}_c,3^j) = \frac{1}{3}+\frac{2}{3^j}+\frac{1}{3^j}\sum_{k=1}^{j-1}\frac{3^{k-1}}{k+1}. \quad (3.6)$$

As $j\to\infty$ the second term on the right converges rapidly and the third term can also be shown to vanish also by replacing the sum by an integral and using l'Hôpital's rule. So

$$\lim_{j\to\infty}\alpha_B(\mathbf{r}_c,3^j) = 1/3, \quad (3.7)$$

and therefore $\overline{\alpha}$ for the corner site[33] of the snowflake is 1/3, which is less than $D_{\mathscr{S}}-1 = \log 5/\log 3 - 1$. In fact, exact calculations of the lattice average of $\alpha(l)$ up to $l=5$ extrapolate to $0.41\ldots < D_{\mathscr{S}}-1$.[34] It seems that $\langle\alpha\rangle_{\mathscr{S}}$ is less than $D_{\mathscr{S}}-1$, the mean-field value, because $\log_t A(\mathbf{r},t)$ is very small very often on $\mathscr{S}$. In general, such a discrepancy will arise when there is an infinite gap hierarchy on the supporting fractals so that the mean-field exponent relation is never achieved even at arbitrarily large distances. *But* the mean-field result $\alpha = D-1$ does hold if we assume that the instantaneous value $\alpha(\mathbf{r},t)$ is constant; this result is expected on lattices which Gefen *et al.*[35] describe as "arbitrarily close to translational invariance," i.e., fractals for which the surface-growth-exponent distribution $F(\alpha)$ is the Heaviside function, and the lacunarity vanishes.

The large fluctuations in A are evident in Figs. 3 and 4 which show corner-site growth on $\mathscr{S}$ and $\mathscr{C}$. Figure 3 shows an exact calculation of $A_{\mathscr{S}}(\mathbf{r}_c,t)$ from a seed at a corner site $\mathbf{r}_c$ on the snowflake $\mathscr{S}(5)$. Notice how often A takes very low values ($=1$). A basic recursion pattern $\{1,1,3\}$ in the A population underlies this times series $A_{\mathscr{S}}(\mathbf{r}_c,t)$. This *coherence* effect also appears eventually in growth from seeds at any site due to the exact, recursive structure of the snowflake. For comparison, Fig. 4 shows $A_{\mathscr{C}}(\mathbf{r}_c,t)$ for growth from a corner seed on the carpet $\mathscr{C}(5)$. No clear recursive pattern is detectable in this time series, in spite of the fact that it represents deterministic growth from a point of high symmetry on an exact fractal. The reason is that activity spreads in a complicated way along the many possible paths on the carpet. This induced randomness also shows itself in the increasing complexity of the algorithm require for an exact, recursive calculation of $A_{\mathscr{C}}(\mathbf{r}_c,t)$ on the carpet.[27,28]

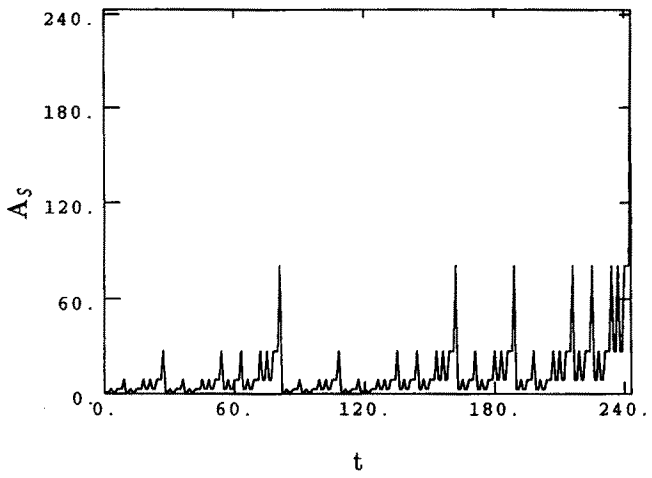

FIG. 3. Plot shows calculated active population $A_{\mathscr{S}}(\mathbf{r}_c,t)$ vs t for growth from corner seed at $\mathbf{r}_c$ on $\mathscr{S}(5)$. Time series is exactly self-similar, obeying scaling law: $A_{\mathscr{S}}(\mathbf{r}_c,\lambda t) = \lambda A_{\mathscr{S}}(\mathbf{r}_c,t)$, for $\lambda = 3$, and t a positive integer. Largest peaks scale linearly like t^1, with exponent $1 > D_{\mathscr{S}} - 1 = 0.4650$. However the time average of $\log_t A(\mathbf{r}_c,t)$ which gives the "surface" growth exponent is $1/3 < D_{\mathscr{S}} - 1$ [see Eqs. (3.5) and (3.7)], whereas area under curve $\Sigma_{s=1}^{t} A_{\mathscr{S}}(\mathbf{r}_c,s) = N(\mathbf{r}_c,t)$ increases like $t^{D_{\mathscr{S}}}$. On infinite $\mathscr{S}$, $A_{\mathscr{S}}(\mathbf{r}_c,t)$ returns to 1 infinitely often.

As expected, the summed variable $N(\mathbf{r}_c,t)$ grows as $t^{D_{\mathscr{C}}}$ for the carpet and looks far smoother than A.

Population fluctuations on the boundary $\partial\mathscr{M}$ of a subset $\mathscr{M}$ of $\mathscr{F}$, with origin or center at site $\mathbf{r}$, also appear if the mass $M(=|\mathscr{M}|)$ of the subset is measured "statically" by covering successively larger neighborhoods of a given site with squares. However these "static" boundary fluctuations can easily be calculated recursively for either $\mathscr{S}$ or $\mathscr{C}$, or any exact fractal.[36]

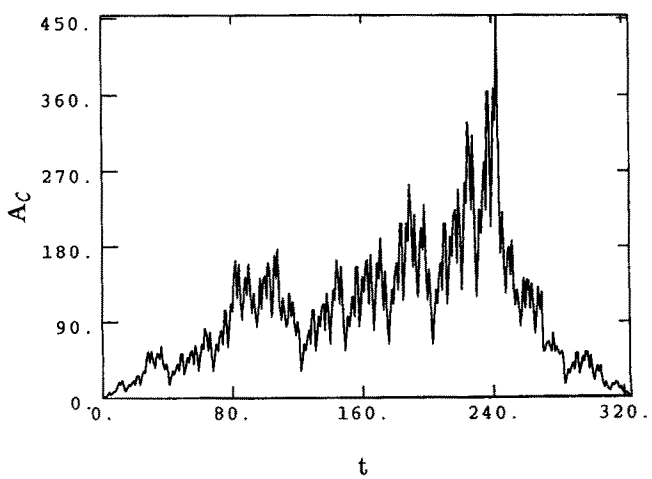

FIG. 4. Plot shows simulated active population $A_{\mathscr{C}}(\mathbf{r}_c,t)$ vs t, for corner seed at $\mathbf{r}_c$ on $\mathscr{C}(5)$. Growth curve $A_{\mathscr{C}}$ shows increasing, random fluctuations, as t increases, with no obvious self-similarity, although CA rule is deterministic, and corner seed is a point of dilatation symmetry of carpet.

IV. GROWTH FOR INITIAL SEEDING FOR CA ON FRACTALS

Growth from a single seed and growth from many, random seeds are related[8,9,37] because the argument of the exponential in the mean-field equations corresponds to the volume swept out by a single site. In the case of a Poisson distribution of seeds, exponentiating this argument is formally equivalent to summing the contributions from many sites by the inclusion–exclusion principle.[38] Also, on a homogeneous lattice every neighborhood is equivalent, so both the single-seed and many-seed growth problems can be exactly solved. But fluctuations increase algebraically with distance on fractals and this produces important deviations from mean-field theory in the initial seeding case. Figure 5 shows six snapshots (a) through (f) of growth, for initial seeding, on a random fractal (decimated to $l=3$ at $p_{\mathscr{S}}=0.5$ and $p_{\mathscr{C}}=0.5$, giving $D=1.77...$). Frame (a) is the lattice state after seeding. Frames (b) through (f) are the lattice states [given by the CA rule (1.1)] at times $t=1,2,...,5$. Here, and in all other pictures of the lattice state, A sites are black, R sites are thick-edged squares, and Q sites are white squares. Even on these small lattices the raggedness of the growing front is apparent,[10] and it is even more obvious on large lattices displayed in color.

A dynamical scaling theory for initial seeding on fractals can be developed as follows. In simulations of this seeding process, a finite realization $\mathscr{F}(l)$ of the (true) fractal $\mathscr{F}=\lim_{l\to\infty}\mathscr{F}(l)$ is seeded with probability p per site, at time $t=1$. Then we *conjecture* that fraction of sites $f_Q(t;p,l)$ that have *always been quiescent* up to time t is given *exactly* by

$$f_Q(t;p,l)=\langle q^{|\mathscr{N}(\mathbf{r},t;l)|}\rangle, \tag{4.1}$$

where

$$q=1-p. \tag{4.2}$$

Equation (4.1) immediately gives

$$f_Q(t;p,l)=q^{N(t;l)}\langle q^{\delta N(\mathbf{r},t;l)}\rangle, \tag{4.3}$$

where

$$\delta N(\mathbf{r},t;l)=N(\mathbf{r},t;l)-N(t;l) \tag{4.4}$$

and

$$N(t;l)=\langle|\mathscr{N}(\mathbf{r},t;l)|\rangle=\frac{1}{|\mathscr{F}(l)|}\sum_{\mathbf{r}\in\mathscr{F}(l)}|\mathscr{N}(\mathbf{r},t;l)| \tag{4.5}$$

is the lattice average of the number of sites $|\mathscr{N}(\mathbf{r},t;l)|$ within radius t of site $\mathbf{r}$. Then Eq. (4.3) reduces to

$$f_Q(t;p,l)=q^{N(t,l)}\sum_{j=0}^{\infty}\frac{(\ln q)^j\langle[\delta N(\mathbf{r},t;l)]^j\rangle}{j!}. \tag{4.6}$$

As $q\to 1^-$ for finite t, or for $\delta N=0$ the homogeneous lattice case, this gives the mean-field result[21]

$$f_Q(t;p,l)=q^{N(t;l)}. \tag{4.7}$$

Exact calculations on the snowflake for $l=3,4$, and 5 suggest the exactness of Eq. (4.1) and the limiting behavior of Eq. (4.7) at low seeding density. For example, up to $l=3$ the evolution on $\mathscr{S}(l)$ can be represented explicitly by a vector of polynomials[39] in q, and for $l=4$ and 5 terms can be enumerated exactly. These results are in excellent agreement with very accurate Monte Carlo simulations of the time evolution. An interesting consequence of the moment expansion (4.6) is that the first p-dependent correction to f_Q is the second moment contribution $\frac{1}{2}(\ln q)^2\langle\delta N(\mathbf{r},t)^2\rangle$ and, in logarithmic plots, this term depresses the growth exponent, i.e., the effective fractal dimension, below the mean-field value D; this is shown by simulation results given later.

This formalism can be extended using a quantitative

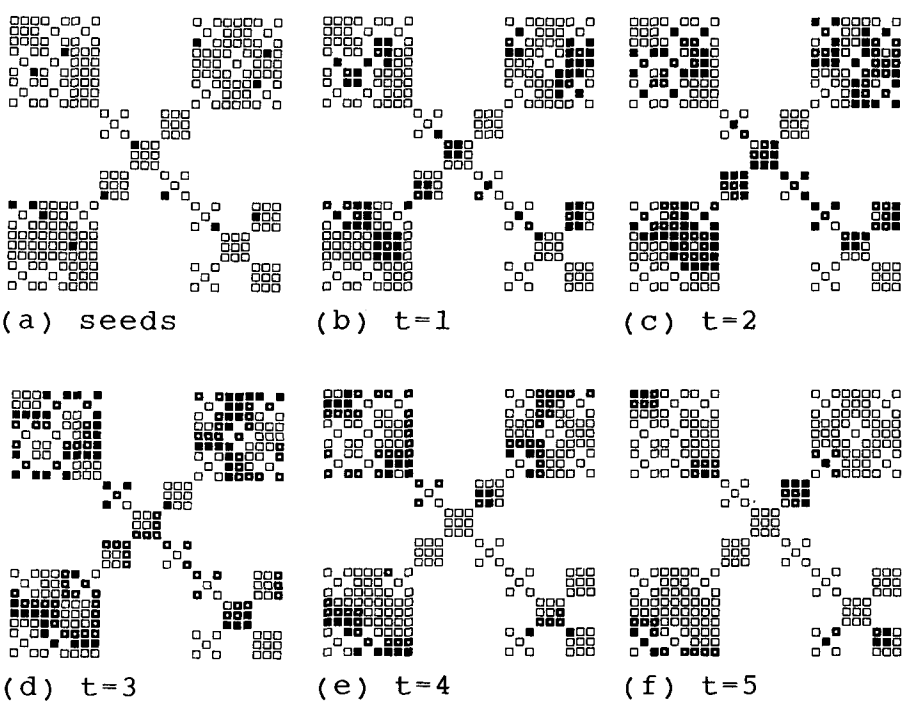

FIG. 5. Six snapshots of time evolution for initial seeding on fractal lattice decimated at $p_{\mathscr{S}}=0.5$ and $p_{\mathscr{C}}=0.5$ giving $D=1.77...$. Frame (a) shows lattice configuration after seeding. Frames (b) through (f) show configuration after rule at successive times $t=1,2,...,5$. Here, and in all other figures of the lattice state, A sites are black, R sites are thick-edged squares, and Q sites are white squares. Note the fragmentation of the wavefronts.

measure of the lacunarity or characteristic hierarchy of gaps in a fractal. After Gefen *et al.*[35] we write the number of sites at *large* lattice contour distance t from site $\mathbf{r}$ as

$$N(\mathbf{r},t) = g(\mathbf{r})t^{D}, \tag{4.8}$$

where $g(\mathbf{r})$ depends only on $\mathbf{r}$. We will assume that $l \to \infty$ for a moment. It is important that in general g has a finite width even as $t \to \infty$ because of the gap hierarchy; only in the limit of vanishing lacunarity is the distribution for g a step function. This ansatz means that

$$\langle N \rangle = \langle g \rangle t^{D}, \tag{4.9}$$

and the central moments are given by

$$\langle [\delta N]^{k} \rangle = \langle [\delta g]^{k} \rangle t^{kD}. \tag{4.10}$$

Using Eqs. (4.9) and (4.10) in Eq. (4.6), as $l \to \infty$, gives f_{Q} on $\mathcal{F}$ as

$$f_{Q}(t;p) = q^{\langle g \rangle t^{D}} \sum_{k=0}^{\infty} \frac{(\ln q)^{k} \langle [\delta g]^{k} \rangle t^{kD}}{k!}. \tag{4.11}$$

The exact enumerations shown in Fig. 6 confirm that the k th central moment of the snowflake increases with exponent kD, with $D = D_{\mathcal{S}}$. The measured slopes of the graphs of $\ln\langle \delta N^{k}(t) \rangle$ vs $\ln t$ for $k = 2$, 3, and 4: i.e., 3.0, 4.4, and 5.8, compare very well with theoretical values ($kD_{\mathcal{S}}$): i.e., 2.93, 4.39, and 5.86. This result implies that mean-field behavior with growth exponent D occurs at early times, but that fluctuations depress this growth exponent below D at slightly later times due to the second moment contribution. This effect should be contrasted with growth on homogeneous lattices where mean-field theory is exact for Poisson seeding, or with growth on random lattices with a finite maximum gap size where fluctuation effects are "controlled" by the central limit theorem[40] and (through the usual cancellation effect of random errors) grow relatively slowly at distances greater than the gap size.

We characterize the lacunarity amplitudes $g(\mathbf{r})$ with a distribution function G defined as follows:

$$G(\gamma) = \lim_{l \to \infty} G(\gamma,l) = \lim_{l \to \infty} \frac{1}{|\mathcal{F}(l)|} \sum_{\mathbf{r} \in \mathcal{F}(l)} \theta[\gamma - g(\mathbf{r};l)], \tag{4.12}$$

which implies the central moments of N can be written as

$$\langle [\delta N(\mathbf{r},t;l)]^{k} \rangle = t^{kD} \int_{-\infty}^{+\infty} (\gamma - \bar{\gamma})^{k} dG(\gamma;l), \tag{4.13}$$

where

$$\bar{\gamma} = \bar{\gamma}(l) = \int_{-\infty}^{+\infty} \gamma dG(\gamma;l). \tag{4.14}$$

The amplitude g for any site $\mathbf{r}$ is given by

$$g(\mathbf{r}) = \lim_{t \to \infty} g(\mathbf{r},t) = \lim_{t \to \infty} t^{-1} \sum_{s=1}^{t} N(\mathbf{r},s) s^{-D}, \tag{4.15}$$

but in practice large t values are satisfactory for estimating g. The lattice averages can be expressed in terms of the distribution G. The shape of the lacunarity distribution $G(\gamma;l)$ is dependent in an important way on lattice topology. Figure 7 shows this for the snowflake and carpet. On $\mathcal{S}(5)$ a large fraction of topologically similar sites lie near the ends of the (tree) branches and these have small amplitudes $g(\mathbf{r})$, so $G_{\mathcal{S}}$ rises sharply at small γ. However, there are many different site topologies with a large number of near neighbors [large $g(\mathbf{r})$] and so G increases to unity smoothly at large γ. Conversely, on $\mathcal{C}(5)$, many sites lie near small holes and few sites near large ones, so $G_{\mathcal{C}}$ rises smoothly at small γ and stops abruptly at large γ. For mixed fractals, G tends to change smoothly at both small and large γ. Monte Carlo estimates of G using the formula (4.12) confirm this description.

In principle it is possible to construct fractals of some chosen D so that the gaps "look" small, i.e., the fractal has vanishing lacunarity and is arbitrarily close to being translationally invariant.[35] In this case the distribution function G is close to the Heaviside step function, and the second and higher central moments for N all become very small. Since

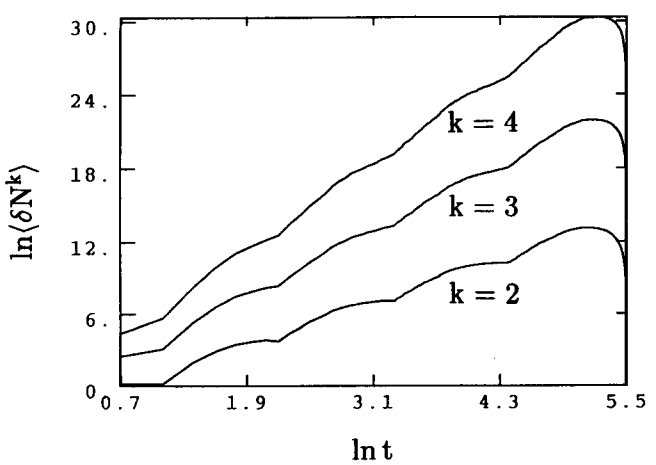

FIG. 6. Exact enumerations of central moments for growth on $\mathcal{S}(5)$ are shown. Graphs of $\ln\langle(\delta N(\mathbf{r},t))^{k}\rangle$ vs $\ln t$ gives slope $kD_{\mathcal{S}} = k \times 1.465...$, i.e., the exponent in Eq. (4.11). For $k = 2$ measured slope is 3.0 and $2D_{\mathcal{S}} = 2.93$; for $k = 3$ measured slope is 4.4 and $3D_{\mathcal{S}} = 4.39$; for $k = 4$ measured slope is 5.8 and $4D_{\mathcal{S}} = 5.86$.

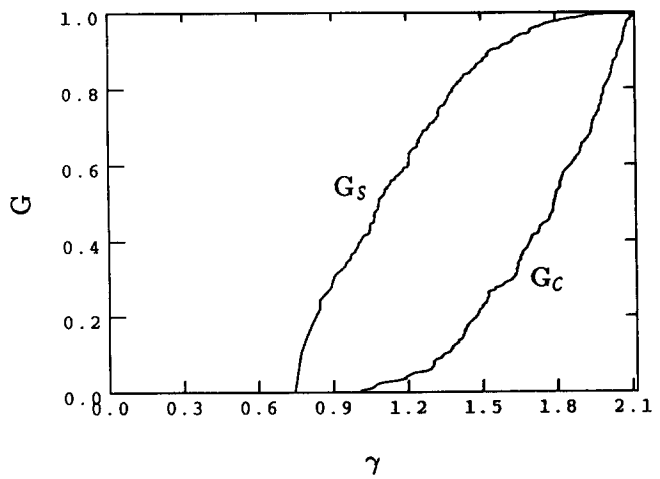

FIG. 7. Graphs of Monte Carlo estimates of lacunarity distributions $G_{\mathcal{S}}(\gamma)$ for $\mathcal{S}(5)$ and $G_{\mathcal{C}}(\gamma)$ for $\mathcal{C}(5)$ are plotted against the lacunarity amplitude parameter γ. $G_{\mathcal{S}}$ rises sharply at small γ because the many "perimeter" sites on $\mathcal{S}$ have few neighbors. $G_{\mathcal{C}}$ rises sharply at large γ because the many sites round small holes in $\mathcal{C}$ have many neighbors.

this means that $\langle N(\mathbf{r},t)\rangle$ depends only on t and not $\mathbf{r}$, the time evolution is described by the first mean-field factor in Eq. (4.3), so that these translationally invariant fractals should behave (in many important respects) like homogeneous lattices.

Another interesting effect can arise from the existence of definite scaling length λ in $\mathcal{F}$.[41] This effect depends on connectedness: It is suppressed on sponge-like structures, like the carpet, but is pronounced on trees like the snowflake. The effect shows itself as structure in the eventual decay of f_Q to zero and is intimately connected with the *coherent* fluctuations on $\mathcal{S}$ in the spreading of wavefronts from single sites discussed earlier. It can be understood in a formal way by writing the scaling ansatz

$$N(\lambda t) = \mu N(t), \tag{4.16}$$

which relates λ (distance) and μ (mass) scaling in the hierarchical structure of $\mathcal{F}$. The smoothest solution of Eq. (4.16) is the mean-field result

$$N(t) \sim t^{D} = t^{\log\mu/\log\lambda}, \tag{4.17}$$

but there are infinitely many other solutions of the functional equation (4.16), and these allow different dynamical symmetries in the time evolution.

These ideas can be examined by extracting an effective fractal dimension D_{eff} from logarithmic plots: Using Eq. (4.17) in Eq. (4.7) gives

$$\log\log_q[f_Q(t;p)] = D_{\text{eff}}\log t + \text{const}, \tag{4.18}$$

where D_{eff} is smooth for *continuous* dilatation symmetry of $\mathcal{F}$. But discrete static, lattice scaling also allows *discrete* dynamic scaling, where λ and μ enter separately into the growth law, and argument from Eq. (4.16) suggests that f_Q is invariant under the discrete scaling transformation

$$p \to p/\mu, \quad \text{and } t \to \lambda t. \tag{4.19}$$

At high seeding density this reflects the discrete, local structure of the lattice. At low seeding density it indicates how, at long times and large distances, the scaled history of growth goes through the same structured phases, as the high-density, local time evolution, because of the self-similarity of $\mathcal{F}$ under dilatation by λ. On logarithmic plots, this discrete dynamical scaling means $f_Q(t;p)$ has the following property:

$$\log\log_q f_Q(t;p) + \log\mu = \log\log_q f_Q(\lambda t;p/\mu), \tag{4.20}$$

so that the graph of $\log\log_q f_Q$ vs $\log t$, is shifted by the vector $\{\log\mu,\log\lambda\}$ for every application of Eq. (4.19). To relate the history of the active wavefronts to the fraction of fresh sites, note that Eqs. (3.1) and (4.7) give

$$f_Q(t-1;p) - f_Q(t;p) = \langle q^{N(\mathbf{r},t-1)} - q^{N(\mathbf{r},t)}\rangle = f_A(t;p), \tag{4.21}$$

where $f_A(t;p)$ is the fractional activity at seeding probability p. Summing Eq. (4.21), using the initial conditions: $f_Q(1;p) = qf_A(1;p) = p$, with $p+q=1$, gives

$$f_Q(t;p) = 1 - \sum_{s=1}^{t} f_A(s;p). \tag{4.22}$$

We now describe Monte Carlo results that support the predictions of fluctuation and discrete symmetry effects on growth for initial seeding. The lattice is randomly seeded at probability p with active sites at time $t=1$. From this state active wavefronts spread on the fractal, progressing from birth to death: Under the CA rule Eq. (1.1) active fronts propagate, and annihilate when they meet, leading to eventual extinction. Our main observation, described below, is that on the sponge-like carpet, both f_A and f_Q change smoothly, whereas on the tree-like snowflake they are structured.

Because $\mathcal{S}$ is a tree with a discrete dilatation symmetry, the (ensemble) activity f_A does not grow smoothly but is spiky at all p: Dynamics is dominated by the passage of the wavefronts through the hierarchy of articulation points much like growth from single seeds. Even the summed variable $f_{\mathcal{S}Q}(t;p) = 1 - \Sigma f_A$, shows these structured, discrete-symmetry effects. Figure 8 illustrates this: Graphs of $\ln\log_q[f_{Q\mathcal{S}}(t;p)]$ vs $\ln t_D$ for $D = D_{\mathcal{S}}$, are shown at p values scaled by $\mu = \mu_{\mathcal{S}} = 5$. Here t_D is a scaled time used to eliminate small distance effects.[42] The initial slopes D_{eff} are all close to $D_{\mathcal{S}} = 1.4650$, consistent with the prediction of mean-field behavior at early times and low seeding density. However these graphs drop smoothly below this average rate of growth ($D_{\text{eff}} < D$) due to the second moment contribution, and eventually tail to the right with wildly fluctuating slopes ($D_{\text{eff}} \gtrless D$) due to higher moment contributions. Each structured tail is similar in shape, corresponding to the discrete symmetry implied by Eqs. (4.19) and (4.20) and can be brought into coincidence[43] with its immediate neighbors by translation through the vector $\{\pm\ln\mu_{\mathcal{S}}, \pm\ln\lambda\} = \{\pm\ln 5, \pm\ln 3\}$.

In contrast, on sponge-like fractals like $\mathcal{C}$, many paths connect remote points, but only the shortest paths contribute to first-passage propagation. As discussed in Sec. III,

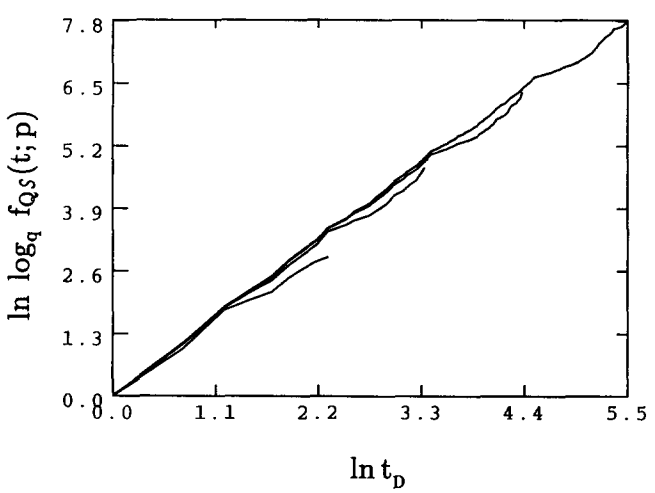

FIG. 8. Initial seeding results are plotted as $\ln\log_q f_{Q\mathcal{S}}(t;p)$ vs $\ln t_D$, where $f_{Q\mathcal{S}}(t;p)$ is fraction of fresh (Q) sites on $\mathcal{S}$(5), and t_D is a scaled time (Ref. 41) with $D = D_{\mathcal{S}}$. Results are averages of 500 runs at four initial seeding probabilities p, scaled by $\mu_{\mathcal{S}} = 5$: $\alpha\sim 0.5$; $\beta\sim 0.1$; $\gamma\sim 0.02$; $\delta\sim 0.004$. For all p, initial slope is $D_{\text{eff}} = 1.44\ldots$, close to mean-field value $D_{\mathcal{S}} = 1.4650$. This indicates continuous dynamical symmetry. At intermediate times, plots show predicted depression below the mean-field line $D_{\mathcal{S}}\ln t_D$. Note fluctuations in derivative, at long times, and the invariance of structured tail plots under translation by $\ln\mu_{\mathcal{S}}$ vertically and $\ln\lambda$ horizontally indicating discrete dynamical symmetry. Cf. Fig. 9.

multiple connectedness causes random fluctuations in growth from isolated site, but for many seeds these *incoherent* fluctuations average out and the total activity varies smoothly. This is apparent in Fig. 9 which shows $\ln \log_q [f_{Q\mathscr{C}}(t;p)]$ vs $\ln t_D$ for $D = D_{\mathscr{C}}$,[42] and three p values scaled by $\mu = \mu_{\mathscr{C}} = 8$. The initial slope of the graph is $D = 1.89...$, close to the mean-field result, $D_{\mathscr{C}} = 1.8928$, as expected at early times; the growth exponent is depressed below this mean-field value at intermediate times and the graphs have only weakly structured tails.

Simulations on hybrid fractals with known D, formed by mixing $\mathscr{S}$, $\mathscr{C}$, and $\mathscr{L}$ generators, when plotted like Figs. 8 and 9, give initial slopes of the corresponding known D.[44]

V. CONTINUOUS SEEDING ON FRACTAL AND HOMOGENEOUS LATTICES

Continuous seeding in wave propagation processes has been modeled on a linear lattice.[24] Continuous nucleation implies an irreversible phase change because new seeds arise only in the untransformed phase, so the equilibrium state is (trivially) the transformed phase. Relaxation to this transformed state shows dynamical scaling.

In contrast, we consider continuous seeding for chemical wave propagation, where seeding occurs at a rate p per lattice site per unit time, so new seeds arise in regions previously swept out by active wavefronts. This is an open, driven system with a nontrivial steady state; indeed, different situations can arise, depending on seeding rate and lattice topology.

For very large $p \in (0.7,1.0]$ all lattices behave similarly since the seeding step saturates the lattice. At intermediate $p \in (0.2,0.7]$, distances between seeds are comparable with the lattice spacing so that waves do not really propagate; hence the CA rule affects nearest neighbors only and the seeding process still dominates behavior. For small $p \in [0,0.2]$, behavior depends on whether lattice neighborhoods support (self-sustaining) oscillators, since continuous seeding generates such oscillators through collisions of seeds with wavefronts. For example, the carpet supports oscillators, whereas the snowflake does not; on random fractals only parts of the lattice will be able to support oscillators, and this leads to interesting effects.

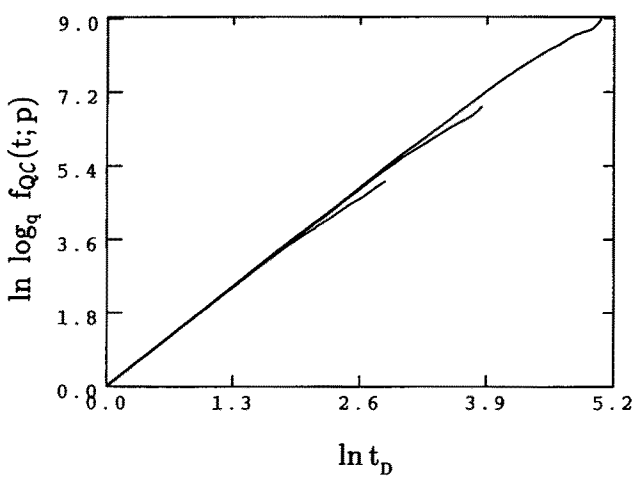

FIG. 9. Initial seeding results are plotted as $\ln \log_q f_{Q\mathscr{C}}(t;p)$ vs $\ln t_D$, where $f_{Q\mathscr{C}}(t;p)$ is fraction of fresh (Q) sites on $\mathscr{C}(5)$, and t_D (at $D = D_{\mathscr{C}} = 1.8928$) is a scaled time (Ref. 41). Results are averages of 50 runs at three initial seeding probabilities p, scaled by $\mu_{\mathscr{C}} = 8$: $\alpha \sim 0.1$; $\beta \sim 0.0125$; $\gamma \sim 0.001\,562\,5$. Plots are smooth, initial slope is $D_{\text{eff}} = 1.89.. \approx D_{\mathscr{C}} = 1.8928$. Dynamical symmetry is nearly continuous for all time, but at long times shows depression of weakly structured tails below mean-field value. Cf. Fig. 8.

The simplest model of continuous seeding is a Markov chain (MC) with two stochastic matrices: $\hat{S}$ represents seeding and $\hat{R}$ the CA rule.[24] These operate successively on the state vector for the system. Since each lattice may have three states this vector has three components, representing the fraction of sites in each of the CA states. The operator $\hat{S}$ expresses the fact that only Q sites can be excited and is strictly time independent:

$$\hat{S}(p) = \begin{pmatrix} 1 & 0 & 0 \\ 0 & 1 & 0 \\ p & 0 & q \end{pmatrix}. \tag{5.1}$$

The transition probabilities of $\hat{R}$ depend on the instantaneous state of the lattice and so change with time, but they may be taken to be time independent, which usually means they are fixed at values appropriate for an initially quiescent lattice. Both models are useful, so to be general we define $\hat{R}$ by

$$\hat{R}(t;p) = \begin{pmatrix} 0 & 1 & 0 \\ 0 & 0 & 1 \\ 1-(1-a_S)^n & 0 & (1-a_S)^n \end{pmatrix}, \tag{5.2}$$

where $n = \langle N(\mathrm{r},1)\rangle - 1$ the lattice mean nearest-neighbor number,[45] and a_S is the active population after seeding. The time evolution is then written as

$$\pi_S(t+1) = \pi_R(t)\hat{S}(p) \tag{5.3}$$

and

$$\pi_R(t) = \pi_S(t)\hat{R}(t;p). \tag{5.4}$$

We denote the steady state in this model by $\{\pi_S^*, \pi_R^*\}$, where $\pi_S^* = (a_S^*, r_S^*, q_S^*)$, etc.

The steady-state fractional activity a_S^* for $\mathscr{L}$ and $\mathscr{S}$ is shown in Fig. 10. For $\mathscr{L}$, $n = 8$ and the time-dependent MC with $a_S = a_S(t)$ gives curve (β) which compares very well with the simulation (α). Note that this nonlinear model predicts that $a_S^* \approx 1/3$ as $p \to 0^+$. Since $\mathscr{L}$ supports self-sustaining patterns under continuous seeding, the time-dependent MC captures the effect of persistent oscillator patterns. This autocatalysis is a singular perturbation or growth instability in the model, since $p = 0$ means $a_S = 0$. For $\mathscr{S}$, $n = 2$ and both time-dependent and time-independent MCs were studied.[45] At large p, the time-dependent MC gives curve (γ) which is very close to the simulation curve (δ), but breaks down at small p because it predicts finite activity at vanishingly small seeding rate. However the time-independent MC, with fixed active population $a_S = a_S(1) = p$ in $\hat{R}$, gives curve (ϵ) which implies the active population $a_S^* \to 0$, as $p \to 0$, like the simulation (δ). Note however that the singular slope found in simulations is not predicted. Since $\mathscr{S}$ cannot support oscillators, we infer the time-independent

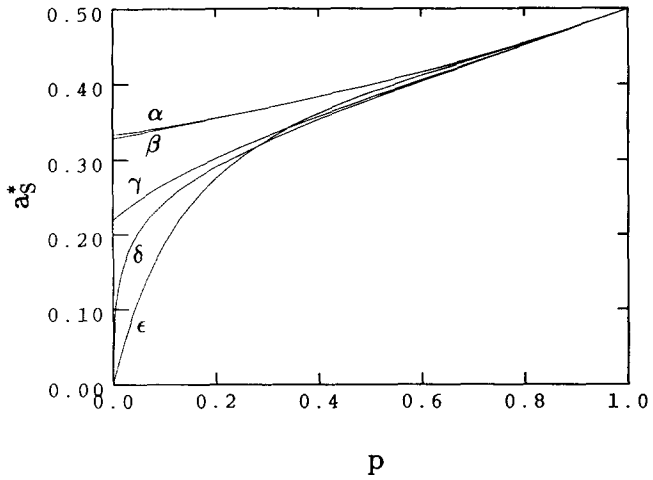

FIG. 10. Comparison of results of Markov chain (MC) models and simulation. Figure shows values of steady-state activity a_S^* vs p, the continuous seeding probability, for $\mathscr{S}$ and $\mathscr{L}$. For $\mathscr{L}$ (upper two curves), α labels simulation, and β time-dependent MC result. These differ slightly at small p where simulation result is 1/3, and at large p results are indistinguishable. Steady state contains self-sustaining pattern at all p on $\mathscr{L}$. For $\mathscr{S}$ (lower three curves), γ is time-dependent MC, δ is simulation, and ϵ is time-independent MC. Note how well simulation and time-dependent MC agree at large p, but simulation and time-independent MC both vanish at small p, because there are no self-sustaining patterns on $\mathscr{S}$. Simulation has infinite derivative at $p = 0$.

model imitates this property better at small p.

It is evident from Fig. 10 that for $p > 0.3$ behavior is independent of lattice structure; at very large p, relaxation to the steady-state shows period 2 oscillations which changes to period 3 as p decreases to intermediate values.[24]

We now discuss pattern morphology for continuous seeding at small p, both on lattices like $\mathscr{L}$ and $\mathscr{C}$ that support oscillators, and also on lattices like $\mathscr{S}$ that only allow transient patterns. We also discuss new propagation effects on random fractals which have mixed neighborhoods.

At small p, all lattices that can support oscillators behave in the same way, regardless of embedding dimension d or fractal dimension D. Pattern formation on these lattices from an initially quiescent field follows the same sequence. This evolution is illustrated in Fig. 11 which shows a history of continuous seeding at *low* seeding rate $p = 0.01$ on the square matching lattice $\mathscr{L}(3)$. Starting from the quiescent lattice, frame (a) at $t = 1$ shows the sparse active state just after seeding. A system of expanding, colliding rings then forms, reminiscent of initial seeding. Frame (b) at $t = 5$ shows this transient ring system. An oscillating center has just formed, as a result of seeding along the active front of the (transient) rings. Frame (c) at $t = 15$ shows target patterns radiated by a variety of (four) oscillators. New oscillators can be formed in both the transient ring system, leading to new target patterns, or in the target pattern system leading to embedded target patterns. Thus the fraction of the lattice taken over by target patterns obeys the continuous nucleation equation (1.3). Roughly one third of the lattice is now in each state A, R, and Q, and this equilibrium population persists through the next stages of pattern evolution. The rate of spontaneous oscillator formation increases with p. Frame (d) at $t = 50$ shows the incipient break up of these target patterns, with an increasing number of new oscillating centers replacing old ones. From now on there is a progressive break down of spatial correlations in the pattern. Frame (e) at $t = 200$ shows an advanced stage of this fragmented but self-sustaining lattice state. Frame (f) at $t = 500$ indicates the statistical invariance of the steady state achieved in frame (e).

The carpet, like $\mathscr{L}$, has a local lattice topology that supports oscillators: This is illustrated in Fig. 12, which shows $\mathscr{C}(4)$ for $p = 0.01$ at $t = 500$. The similarity to frame 11(f) is evident.

In contrast, $\mathscr{S}$ (a simple tree) cannot support oscilla-

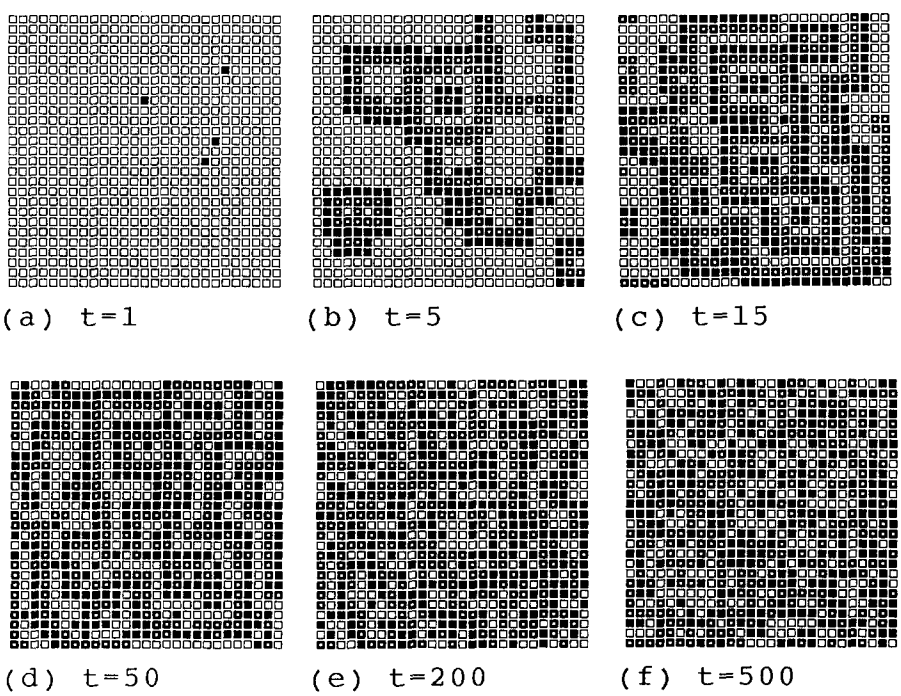

FIG. 11. Snapshots of the time evolution on the continuously seeded square-matching lattice $\mathscr{L}(3)$. (a) At $t = 1$, the initially seeded state is shown. (b) At $t = 5$, transients rings with one oscillator have formed. (c) At $t = 15$, several oscillators have formed and radiate rings; population is 1/3 in A, R, and Q. (d) At $t = 50$, the continuous formation of oscillators has reduced correlation length of wavefront. (e) At $t = 200$, the ring structure has completely broken up. (f) At $t = 500$, the steady state is statistically the same as (e).

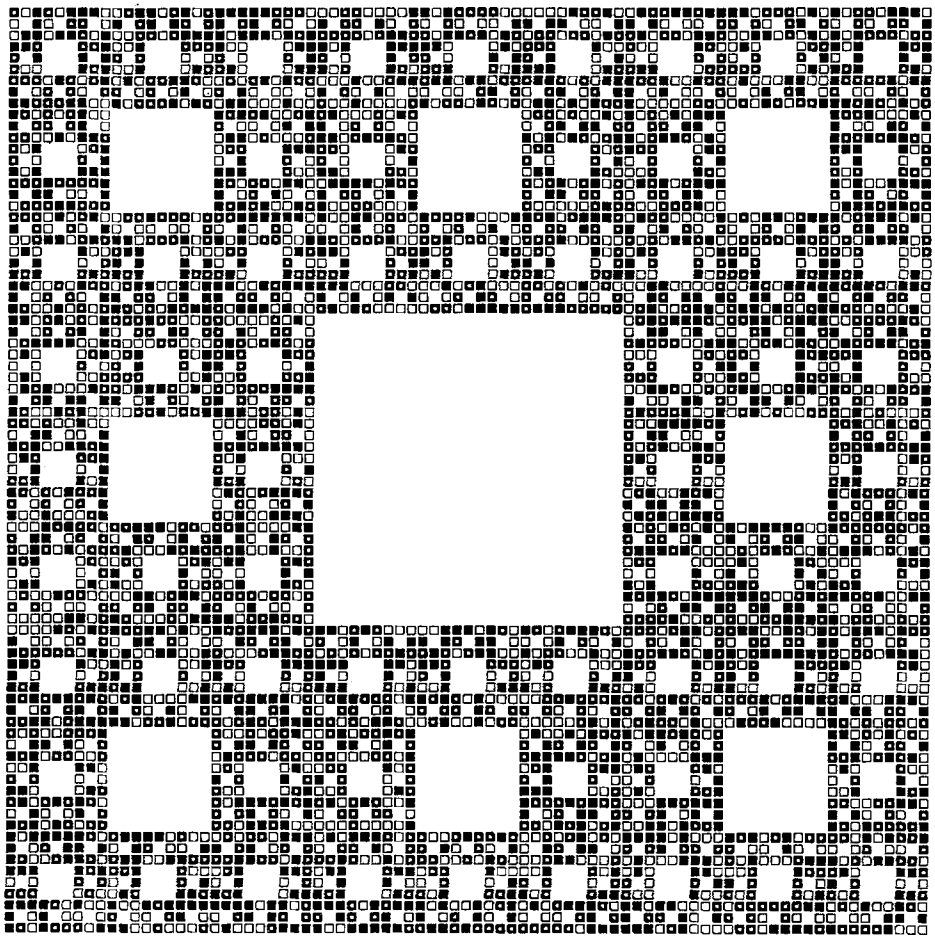

FIG. 12. Steady state on carpet $\mathscr{C}(4)$ at $t = 500$ for continuous random seeding at $p = 0.01$. Note that roughly 1/3 of lattice sites are in each state A, R, and Q. Cf. Fig. 13 for $\mathscr{S}(4)$.

tors, and must be continuously seeded to sustain activity. Figure 13 shows $\mathscr{S}(4)$ at $t = 500$ continuously seeded at $p = 0.01$. Notice how sparse activity is compared to that on $\mathscr{L}$ [Fig. 11(f)] and $\mathscr{C}$ at the same time. Figure 10 shows $a_S^* \to 0$ as $p \to 0$ with infinite derivative, so a_S^* should show fractional power-law scaling at very small p. This means activity after $\hat{S}$ or $\hat{R}$ is very similar, and so we denote this steady-state population by $f_A^*(p)$. Furthermore, relaxation to this steady state should show scaling behavior. We now present a mean-field argument to find the dynamical scaling exponents for $\mathscr{S}$. To be more general, let $f_A^*(p)$ denote the steady-state fraction of active sites on any fractal $\mathscr{F}$, which like $\mathscr{S}$, supports only transients patterns. Then $t_{1/2}^*(p)$ will denote the time for $f_A(t;p)$ to increase to $f_A^*/2$ when the initial state is quiescent. At seeding rate p, every seed is surrounded, on average, by a volume $V_{\mathscr{W}}$ proportional to p^{-1} ($pV_{\mathscr{W}} = 1$) in the "world" $\mathscr{W} = \mathscr{F} \times \{t\} \subset \mathscr{R}^d \times \{t\}$. Thus distance and time for $V_{\mathscr{W}}$ scale like $t(p) = p^{-1/(D+1)}$, where $t(p)$ is the scaling distance/time at seeding rate p. Now the mass in $\mathscr{F}$ swept out in time $t(p)$ scales like $t(p)^D$ so the density in $V_{\mathscr{W}}$ scales like $t(p)^D / t(p)^{D+1} = t(p)^{-1} = p^{1/(D+1)}$, i.e.,

$$f_A^*(p) = \lim_{t \to \infty} f_A(t;p) \propto p^{1/(D+1)}, \tag{5.6}$$

since f_A is the time average of the mean activity per lattice site. The proportionality constant will depend on the particular realization when $\mathscr{F}$ is a random fractal. Similarly, the relaxation time to saturation $t_{1/2}^*(p)$, scales like

$$t_{1/2}^*(p) \propto p^{-1/(D+1)}. \tag{5.7}$$

For the case studied, $\mathscr{F} = \mathscr{S}$, the steady-state population exponent $(D_{\mathscr{S}} + 1)^{-1}$ is 0.406..., whereas simulations for seven p values between 10^{-4} and 10^{-2} give a steady-state exponent of 0.39 ± 0.02.[46] For the same range of p, simulations show the relaxation time $t_{1/2}^*(p)$ scales with exponent -0.42 ± 0.02. So this simple scaling theory works quite well.

On mixed fractals even richer dynamics is observed: Fig. 14 shows a fractal $\mathscr{F}$ ($p_{\mathscr{S}} = 0.9, p_{\mathscr{C}} = 0.1$) which was continuously seeded at $p = 0.02$ from $t = 1,2,\ldots,20$. Seeding then stopped giving the pattern shown at $t = 200$. Period 3 and period 4 signals propagate along the tree branches, separated by carpet fragments containing oscillators. Interestingly, period 3 does not "eat up" period 4 as on a homogeneous lattice and the whole configuration has period 12.

VI. DISCUSSION

A cellular automaton growth model of the spread of excitation in fractal spaces has been presented. The local CA rule imitates the propagation of localized activity, so the model is an epidemic process with certain spread of infection between neighbors, like a forest fire where every tree is inflammable! The underlying fractal lattices display differences in connectedness and fractal dimension that occur in

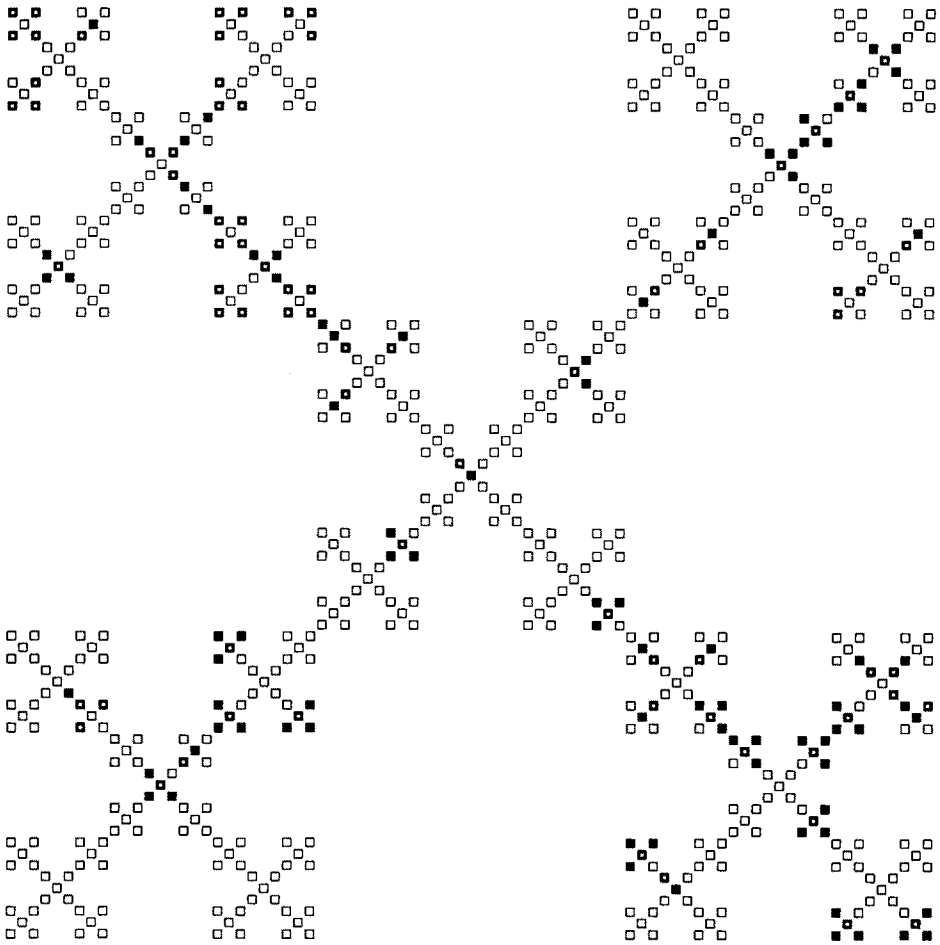

FIG. 13. Steady state on snowflake $\mathscr{S}(4)$ at $t = 500$ for continuous random seeding at $p = 0.01$. Note low density of active sites since no oscillators can be formed. Cf. Fig. 12 for $\mathscr{C}(4)$.

microscopic and macroscopic natural spaces. The way in which the structure of the fractal supporting CA growth affects dynamics has been examined carefully.

For single seeds the instantaneous activity does not grow smoothly with the mean-field exponent $D-1$, but shows very large fluctuations (like random voltages across percolation clusters). The average growth exponent may also be "renormalized" from $D-1$ because of the infinite correlation length of fractal gaps. On trees with a scaling length, fluctuations are structured and produce similar scaling peaks in the active population; however, on very spongy (highly ramified) fractals (or even on exact fractals like the carpet) the instantaneous activity is intrinsically random. This is in marked contrast to homogeneous lattices where growth from single seeds is smooth and predictable.

In initial seeding, where seeds are randomly scattered on the lattice, the area swept out by the excitation should depend only on fractal dimension D in the mean-field approximation. At low seeding density and early times this growth law is true on fractals, but lattice fluctuations are important at longer times and (at first) depress the growth exponent below the mean-field value. On trees with a scaling length a discrete dynamical symmetry appears even in ensemble growth at high seeding density or long times, due to the hierarchical gap structure. An important implication of the model is this: Wild fluctuations in the active population may be unrelated to the population of previously active (infected) sites, and therefore do not measure the progress of disease or reaction on a tree-like structures; however, this activity is correlated with "damage" or "disease" on sponge-like fractals. Therefore, if activity promotes an immune response in living systems, the model suggests that such a response will be correlated with the degree of infection in a way that depends on the connectedness of the structure involved.

In continuous seeding, lattice structure again plays a crucial role. If a lattice can support oscillators, it is eventually filled with random periodic patterns, whose population is easily predicted by a nonlinear time-dependent Markov chain. However, if the lattice is a tree it cannot support oscillators, and populations scale with seeding density. Random fractals show complicated periodic effects due to the oscillator-sustaining properties of different lattice regions. The phenomena described here are easily generated by random seeding on fractals with simply connected branches and multiply connected (oscillating) nodes, because periodic pulses can propagate along the branches between the nodes. In view of the universal computing capability of some CA, and the fact that the CA studied here imitates an excitable medium, it seems very likely that even richer behavior with a logical or computing function can be found in this dynamical model.

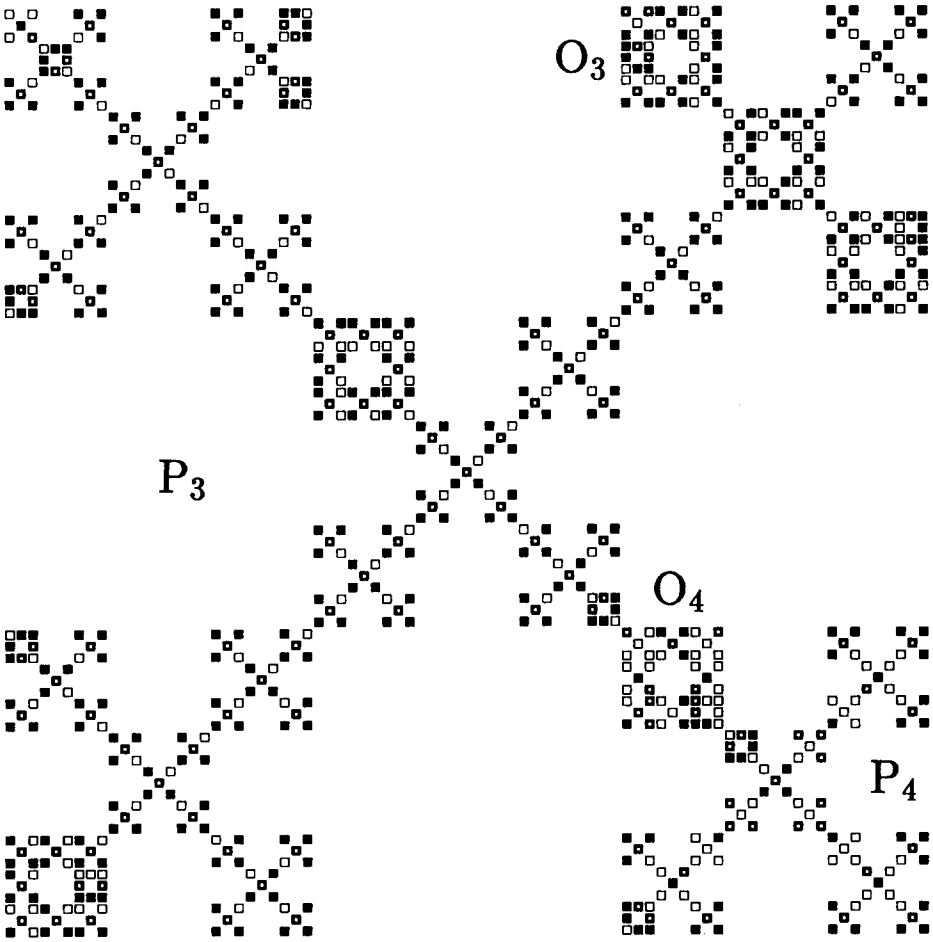

FIG. 14. Steady state on largely tree-like fractal seeded for first 20 time steps. The lattice state is shown at $t = 200$. The configuration has period 12 because it contains period 3 and period 4 oscillators. Signals propagate along tree-like limbs between carpet oscillators nodes. A period 4 oscillator O_4 separates the upper left, period 3 region P_3 from the lower right, period 4 region P_4. Region P_3 is driven by oscillator O_3. Oscillator O_4 is not destroyed by incident period 3 waves. Coexistence of different periods (in the CA) is allowed on fractals but forbidden on homogeneous lattice.

ACKNOWLEDGMENTS

This work was supported by the Natural Sciences and Engineering Research Council (NSERC) of Canada. We would also like to thank Mark Bradley and Ray Kapral for preprints on theoretical work, and Jerzy Maselko and Ken Showalter for interesting conversations about experiments.

[1] See, e.g., J. W. Christian, *The Theory of Transformations in Metals and Alloys* (Pergamon, Oxford, 1975).

[2] See articles in *Oscillations and Travelling Waves in Chemical Systems*, edited by R. J. Field and M. Burger (Wiley, New York, 1985).

[3] B. P. Belousov, Sb. Ref. Radiat. Med., Moscow **1958**, 145 (1959).

[4] A. M. Zhabotinsky, Dokl. Akad. Nauk SSSR **157**, 392 (1964).

[5] See, e.g., S. Wolfram, Rev. Mod. Phys. **55**, 601 (1983), and articles in Physica D **10** (1984).

[6] B. B. Mandelbrot, *The Fractal Geometry of Nature* (Freeman, New York, 1983).

[7] See, e.g., A. L. Goldberger, D. R. Rigney, and B. J. West, Sci. Am. **262**, 40 (1990).

[8] Invasion percolation, the propagation of forest fires (first-passage propagation) and the general epidemic process are all related to the propagation process described here. See, e.g., N. T. J. Bailey, *The Mathematical Theory of Infectious Diseases* (Griffin, London, 1975); D. Wilkinson and J. F. Willemsen, J. Phys. A **16**, 3365 (1983); P. Grassberger, Math. Biosci. **63**, 157 (1983); T. Ohtsuki and T. Keyes, Phys. Rev. A **33**, 1223 (1986); Y. Li, W. G. Laidlaw, and N. C. Wardlaw, Adv. Colloid Interface Sci. **26**, 1 (1986).

[9] D. Cannell and C. Aubert describe the formation of colloidal silica aggregates in: *On Growth and Form*, edited by H. E. Stanley and N. Ostrowsky (Martinus Nijhoff, Boston, 1986), pp. 187–197; see also other references in this article. D. A. Weitz, D. S. Huang, M. Y. Lin, and J. Sung, Phys. Rev. Lett. **54**, 1416 (1985) have studied colloidal gold aggregates. Such structures could provide microscopic support for phase changes, or chemical transformation reactions on fractal surfaces.

[10] J. Maselko, J. S. Reckley, and K. Showalter, J. Phys. Chem. **93**, 2774 (1989) have studied the BZ reaction with ferroin catalyst immobilized in cation-exchange resin. J. Maselko has investigated wave propagation for random mixtures of catalytic and noncatalytic beads at the percolation threshold, and has seen similar effects to those described here, e.g., the formation of ragged wavefronts (private communication). See also Ref. 31 of this reference. It should be possible to use electrostatically printed, model fractal spaces using a colorless catalytic thermoplastic support material, or attach catalytic beads to a sticky fractal image and observe wave propagation in solution.

[11] J. M. Greenberg, B. D. Hassard, and S. P. Hastings, Bull. Am. Math. Soc. **84**, 1296 (1978); J. M. Greenberg and S. P. Hastings, SIAM J. Appl. Math. **34**, 515 (1978); W. Freedman and B. Madore, Science **222**, 615 (1983).

[12] S. J. Fraser, Phys. Rev. A **38**, 953 (1988).

[13] In $\mathscr{R}^d$, fractal or (strictly) box-counting dimension is measured as $D = -\lim_{\epsilon \to 0} \log N(\epsilon)/\log \epsilon$, where $N(\epsilon)$ is the number of d-dimensional cubes of side ϵ needed to cover the fractal. In practice, fractals are modelled by finite lattices, with inner and outer length cutoffs, so D is an exponent governing mass–length scaling between these cutoffs.

[14] The fractal lattices $\mathscr{F}$ are all topologically connected. "Connectedness" here refers to *tree-like* or *sponge-like* character of $\mathscr{F}$, i.e., the degree of ramification. This depends on the fraction of articulation points in $\mathscr{F}$; see Ref. 6 and Ref. 9 of Ref. 12. Trees are quasi-one-dimensional, or simply connected and every point is an articulation point, so the (degree of) ramification is one. Nonseparable graphs (sponges) are multiply connected, and require (finitely or maybe infinitely) many cuts to separate a given region, depending on whether they are finitely or infinitely ramified. In fact, $\mathscr{C}$ is infinitely ramified. See also F. Harary, *Graph Theory* (Addison-Wesley, Reading, Mass., 1972), Chap.5.

[15] Minimum path is mentioned in K. M. Middlemiss, S. G. Whittington, and D. S. Gaunt, J. Phys. A **13**, 1835 (1980), and a branched-random-

walk model of percolation clusters in Z. Alexandrowicz, Phys. Lett. A **80**, 284 (1980). See also M. Barma, J. Phys. A **18**, l277 (1985) and S. Roux, *ibid.* **18**, L395 (1985), and references therein.

[16] See H. Stanley, in Ref. 17, pp. 21–68, for a discussion of various growth exponents. Other names have been used for d_{chem} and related growth exponents. See, e.g., S. Havlin and R. Nossal, J. Phys. A **17**, L427 (1984); P. Grassberger, *ibid.* **19**, 1681 (1986); R. Rammal, J. C. Angles d'Auriac, and A. Benoit, *ibid.* **17**, L491 (1984).

[17] A. N. Kolmogorov, Izv. Akad. Nauk SSSR, Ser. Fiz. **3**, 355 (1937).

[18] W. A. Johnson and R. F. Mehl, Trans. Am. Inst. Min. Metall. Pet. Eng. **135**, 416 (1939).

[19] M. Avrami, J. Chem. Phys. **7**, 1103 (1939); **8**, 212 (1939); **9**, 177 (1941).

[20] S. Fraser and R. Kapral, J. Chem. Phys. **85**, 5682 (1986); S. J. Fraser, J. Comp. Chem. **8**, 428 (1987). Small corrections to Eqs. (1.3) and (1.4) arise from finite size effects of the nuclei, discrete lattice and time effects, and the choice of initial time.

[21] R. M. Bradley, J. Chem. Phys. **86**, 7245 (1987).

[22] Boundary effects in nucleation have recently been considered by M. Weinberg and R. Kapral, J. Chem. Phys. **91**, 7189 (1989).

[23] The geometry of moving boundaries in nucleation is discussed in R. M. Bradley and P. N. Strenski, Phys. Rev. B **40**, 8967 (1989).

[24] S. J. Fraser and Y. S. Kan, Nucl. Phys. B **5**, 241 (1988).

[25] S. Glasstone, *Textbook of Physical Chemistry* (MacMillan, London, 1960).

[26] Regarded as sets, $\mathcal{N}$ is the union of successive $\mathcal{A}$'s growing out from a given seed. At time t, $\mathcal{N}(t) = \cup_{s=1}^{t} \mathcal{A}(s)$ where $\mathcal{A}(s) \cap \mathcal{A}(s') = \emptyset$, so $\{\mathcal{A}(s) | s = 1(1)t\}$ is a partition of $\mathcal{N}(t)$. Therefore writing $A = |\mathcal{A}|$ gives $N(t) = \Sigma_{s=1}^{t} A(s)$.

[27] The time series for the active front for growth from a corner seed on $\mathcal{S}(l)$ can be calculated recursively. Let $\mathbf{a}_{\mathcal{S}}(l) = \{a_{\mathcal{S}}(t): t = 1(1)3^l\}$ be this time series at decimation level l. The corner time series for the generator $\mathcal{S}(1)$ is the row vector $\mathbf{a}_{\mathcal{S}}(1) = \{1,1,3\}$. The recursion is: $\mathbf{a}_{\mathcal{S}}(l+1) = \mathbf{row}\{\mathbf{a}_{\mathcal{S}}(1)'\mathbf{a}_{\mathcal{S}}(l)\}$ where $'$ denotes transpose and the operator **row** reads the matrix argument row by row into a row vector. The lattice average time series can be obtained by exact enumeration for $\mathcal{S}(5)$. Recursive algorithms for Carpet time series are very complicated, but such procedures for "space" series, parametrized by a length, are simple for both $\mathcal{S}$ and $\mathcal{C}$.

[28] This unpredictability in a deterministic process resembles *Chaos*, because it is *intrinsic*, but it has high-frequency contributions like *extrinsic noise*. See, e.g., article by J. Ford, in *Chaotic Dynamics and Fractals*, edited by M. F. Barnsley and S. G. Demko (Academic, Toronto, 1986), pp. 1–52; G. J. Chaitin, Sci. Am. **259**, 80 (1988). See also Ref. 29.

[29] The CA growth process under study is not stationary, but displays "multifractal" effects determined by particular fractal subsets, e.g., the articulation points. Under steady-state conditions, transport properties with this kind of dependence have been studied. See, e.g., L. De Arcangelis, S. Redner, and A. Coniglio, Phys. Rev. B **31**, 4725 (1985); **34**, 4656 (1986); R. Rammal, C. Tannous, P. Breton, and A.- M. S. Tremblay, Phys. Rev. Lett. **54**, 1718 (1985); R. Rammal, C. Tannous, and A.-M. S. Tremblay, Phys. Rev. A **31**, 2662 (1985); F. M. Bhatti and J. W. Essam, J. Phys. A **19**, L519 (1986); Y. Meir, R. Blumenfeld, A. Aharony, and A. B. Harris, *ibid.* **19**, L791 (1986).

[30] Measures for stationary, ergodic processes, or steady states, with fractal support are considered in T. C. Halsey, M. H. Jensen, L. P. Kadanoff, I. Procaccia, and B. I. Shraiman, Phys. Rev. A **33**, 1141 (1986).

[31] Analysis of fractal time series is discussed in H. Fujisaka and M. Inoue, Prog. Theor. Phys. **78**, 1203 (1987); M. Inoue and H. Fujisaka, *ibid.* **79**, 1251 (1988). The logarithmic form of Eq. (3.2) produces "stationary" time series from algebraically growing ones.

[32] It is convenient to represent averages as Stieltjes integrals since the convergence of the integrator F can be tested in the L^2 norm, whereas the convergence of its "derivative" which is an array of delta functions cannot.

[33] The exponent α for the center site of $\mathcal{S}$ is also 1/3,by a related argument. This value of α also holds for sites of high symmetry in $\mathcal{S}$.

[34] In calculating the averages of α^m from Eq. (3.5), the time t at which the evolution of activity from a given site $\mathbf{r} \in \mathcal{S}(l)$ can depend on both $\mathbf{r}$ and l. The time to cessation of activity $[t_{\text{death}}(\mathbf{r};l)]$, and the time to traverse half the lattice diameter $[t_{1/2}(l)]$ were both tried, and gave very similar results.

[35] Y. Gefen, Y. Meir, B. B. Mandelbrot, and A. Aharony, Phys. Rev. Lett. **50**, 145 (1983).

[36] In the static picture, the covered part of $\mathcal{F}$ is $\mathcal{M}(\mathbf{r},2s+1) = \mathcal{L}(\mathbf{r},2s+1) \cap \mathcal{F}$, where $\mathcal{L}(\mathbf{r},2s+1)$ is a square of side $2s+1$ centered at $\mathbf{r}$, and $M(\mathbf{r},2s+1)$ is the number of sites in $\mathcal{L}$. However $\mathcal{M}$ is need *not* be connected. Since the wavefront moves with unit velocity, the neighborhood $\mathcal{N}(\mathbf{r},s) \subset \mathcal{M}(\mathbf{r},2s+1)$ and therefore $N(\mathbf{r},s) < M(\mathbf{r},2s+1)$. Of course $\mathcal{N}$ is connected.

[37] Suppose the activity spreads across the lattice deterministically with unit velocity, and growth starts at time $t = 1$: Every site lying within distance t of an isolated seed will have been excited by that seed at time t. Round the seed there is an active front (not necessarily connected) of "radius" t, enclosing an area of previously excited sites. Conversely, for many seeds, an initially quiescent site will be still be Q at time t, if and only if all its neighbors within distance t are empty at $t = 1$. For any chosen lattice site these "occupied" and "empty" neighborhoods, of diameter t, are identical. Therefore on a random lattice, the average number of sites in a neighborhood of radius t, determines both growth from single sites, and (through the probability of initial vacancy) growth from random seedings of sites. See also Refs. 18–21.

[38] See, e.g., C. Berge, *Principles of Combinatorics* (Academic, New York, 1971); J. Riordan, *An Introduction to Combinatorial Analysis* (Wiley, New York, 1958).

[39] The $\{1,1,3\}$ recursive pattern characteristic of $\mathcal{S}$ is clearly reflected in the amplitudes and exponents of these polynomials.

[40] W. Feller, *An Introduction to Probability Theory and its Applications* (Wiley, New York, 1968), Vol. I.

[41] A tree of identical elements cannot be embedded in finite dimensional Euclidean space, since volume in such spaces increases algebraically with distance from an arbitrary origin, whereas the space occupied by the tree elements increases exponentially with distance from any site. Trees embeddable in a lattice, must have a decaying distribution of branch lengths. This decay is structured on the snowflake, but may be smooth on a random tree. Growth is affected by this difference.

[42] In order to remove local discrete lattice effects in the plots in Figs. 8 and 9, a scaled time $t_D = a_D t + b_D$ was used. Parameters a_D and b_D were chosen to make $N(1) = a_D + b_D = 1$, and $N(2) = (2a_D + b_D)^D$ correct on both the square-matching lattice where $N(2) = 9$, and the infinite snowflake where $N(2) = 3$. The snowflake value for $N(2)$ was calculated recursively. Other values of a_D and b_D were linearly interpolated.

[43] Care must be taken to weight results according to their generator contributions at the longest length scale, in order to avoid bias at long times.

[44] Strictly speaking, there are structural differences on small scales, but agreement at large scales in these log–log plots. This reflects both the recursive lattice structure and the new site topologies created at each level of decimation.

[45] As $l \to \infty$: For $\mathcal{L}$, $n = 8$ at every site; for $\mathcal{S}$, $n = 2$ from $N(2) = 3$ in Ref. 42.

[46] In Ref. 24 we found that on the 1D lattice the steady-state exponent was approximately 0.44 at the p values tested; this result is depressed below the 1D mean-field value of 1/2.